Final Draft
of the original manuscript:

Lalbeharry, R.; Behrens, A.; Guenther, H.; Wilson, L.:
Matching of Coastal and Open Ocean Wave Models in a Mesoscale Application over Lake Erie
In: Atmosphere - Ocean (2009) University of British Columbia

DOI: 10.3137/OC305.2009

Matching of coastal and open ocean wave models in a mesoscale application over Lake Erie

ROOP LALBEHARRY

Environmental Numerical Weather Prediction Research Section, Science and Technology Branch

Environment Canada,, Toronto, ON M3H 5T4

ARNO BEHRENS

GKSS Research Centre, Institute for Coastal Research, Max-Planck-Strasse 1, 21502 Geesthacht, Germany

HEINZ GUENTHER

GKSS Research Centre, Institute for Coastal Research, Max-Planck-Strasse 1, 21502 Geesthacht, Germany

LAURENCE WILSON

Environmental Numerical Weather Prediction Research Section, Science and Technology Branch

Environment Canada, , Dorval, QC H9P 1J3

Revised version submitted to: *Atmosphere-Ocean*

24 February 2009

Accepted: *18 March 2009*

Published: *September 2009*

Corresponding author's address: Roop Lalbeharry, Environment Canada, Science and Technology Branch, Meteorological Research Division, 4905 Dufferin St., Toronto, Ontario, Canada M3H 5T4

Tel: +416-739-4912. Fax: +416-739-2221

E-mail: Roop.Lalbeharry@ec.gc.ca

Abstract. Three widely used wave models, namely, the open ocean wave model WAM (Cycle-4.5, hereafter referred as WAM4.5) and the coastal models, SWAN (Cycle III version 40.31, hereafter referred as SWAN) and the K-model, are applied to Lake Erie to simulate waves at a spatial resolution of about 4 km. The results of a three-week hindcast study are compared with buoy observations in terms of integrated parameters, one-dimensional (1-D) and two-dimensional (2-D) energy spectra, scatter plots and statistical analyses of the wave fields. The time development of the 1-D spectra by the models match the buoy measurements well. All the wave models tend to overpredict the wave heights and underpredict (particularly the K-model) the peak period. SWAN performs best for the wave heights and WAM4.5 for the peak periods and is computationally less demanding, whereas the spatial resolution applied to Lake Erie seems to be too coarse for an adequate use of the K-model. In general, WAM4.5 shows advantages over coastal wave models in operational intermediate-scale applications.

1 Introduction

The development of wave forecasting models which can predict sea states in a consistent way for all marine activities is a challenging task. Not only do nearshore marine activities require different information on different spatial and time scales than (for example) shipping activities, but also the physical processes which affect wave growth, propagation and decay differ considerably in nearshore areas compared to open ocean areas. The challenge is to build a model which can simulate in a consistent way both nearshore and deep water waves and the transition between these two regimes. Wave modelling in lakes poses similar problems if the lake consists of shallow, transitional and/or deep water areas.

Existing wave models may be specialized in their applicability. For example, the European community model WAM, which is used widely in operational wave forecasting,

was originally developed for deep water only, and is typically applied at relatively low horizontal resolution, with grid lengths greater than 20 km. (WAMDI Group, 1988). Later, the model SWAN was developed, using WAM as a basis, but designed for application in coastal waters (Holthuijsen, 2007; Booij et al., 1999; Ris et al., 1999). This model has been applied at the higher spatial resolution needed for more accurate simulation of the effects of complex shorelines and bottom topography. More recently, a model also derived from WAM, but with a very different structure was developed specifically for application in coastal water conditions at high resolution. This model is called the K-model, because it uses the wave number k instead of the frequency σ as one of the model coordinates (Schneggenburger, 1998; Schneggenburger et al., 2000). These three models are the subject of this paper.

Earlier investigations with WAM Cycle-4.0 (hereafter referred as WAM4) applied to coastal seas or lakes (e.g. Monbaliu et al., 2000; Liu et al., 2002; Soomere et al., 2008) demonstrated that such an open ocean model can perform practically as well as specific coastal wave models in terms of the basic wave parameters such as the SWAN model and the so-called K-model described in Section 2 since these models follow the principles of WAM. Some of the high resolution small-scale enhancements of WAM4 introduced by Monbaliu et al. (2000) have been included in later versions of WAM such as WAM4.5 used in this study.

A very interesting question in terms of wave modelling was raised by Liu et al. (2002) who used a comparison of four different wave models, namely, the WAM4, the Great Lakes Environmental Research Laboratory (GLERL)/Donelan model (Donelan, 1977), the Deep-water Wave (DWAVE; Resio, 1981) and Shallow-water Wave (SHALWV; Hughes and Jensen, 1986) models. They applied these models to Lake Michigan to support their claim that the common wave models based on the concept of a wave energy spectrum may have reached a limit in the accuracy with which they can simulate realistic wave generation and

growth conditions. This point of view is discussed in subsection 3c in the context of the results of the present investigation.

The coastal wave models SWAN and K-model were developed for use in nearshore, highly variable tidal environments (Ris et al. 1999) or lakes of intermediate and shallow water depths. Different previous investigations dealing with comparisons of coastal models (e.g. Lin et al., 2002; Moghimi et al., 2005) provide good benchmarks with regard to the quality of the results that can be expected. Lin (2000), for example, compared the second generation model GLERL/Donelan model with SWAN without including the effects of current and water level variations. In contrast to that Moghimi et al. (2005) took the tidal parameters into account in their comparison of SWAN and the K-model in order to gain insight into the effects of currents and water depths and their influence on the waves.

This study focuses on the comparative evaluation of three wave models in an enclosed water body, Lake Erie. A limited intercomparison of wave models in Lake Erie was carried out by Lalbeharry et al. (2001). This study showed that using only bottom friction and depth refraction in WAM4 improved the forecasts compared to the deep water version of WAM4, especially in high wave activity situations when validated against observations at buoys located in transitional water depths.

For this investigation we have attempted to simplify the comparability of the three wave models by ensuring that the source terms are equivalent in the three models. In this way, the intercomparison can focus on the differences in the formulation of the nearshore and shallow water physical processes, and on the differences in the handling of wave-wave interactions in the models.

The general goal of the work reported in the paper is to evaluate the three models WAM4.5, SWAN and the K-model at high resolution (0.05^{o} grid length which corresponds to about 5.5 km in the north-south direction and 4 km in the east-west direction at the latitude of

Lake Erie) to determine whether a coastal model is required to get reliable results on this scale or whether the ocean model WAM4.5 is capable enough to provide wave data of sufficient and acceptable accuracy and quality. The three different wave models are briefly described in Section 2. Discussions about the wave model results in comparison with buoy measurements and a corresponding statistical analysis are presented in subsection 3c, followed by summary and conclusions in Section 4.

2 Description of the wave models

a *The Action Density Equation*

The ocean waves are described with the two-dimensional wave action density spectrum $N(\sigma,\theta,\phi,\lambda,t)$ as a function of relative angular frequency σ ($= 2\pi f$, f being frequency), wave direction θ, latitude ϕ, longitude λ, and time t. The dispersion relation $\sigma = [(gk)\tanh(kh)]^{1/2}$ relates the angular frequency σ to wave number k ($= 2\pi/L$, L being the wavelength) and water depth h (g is acceleration due to gravity). The action density spectrum is defined as the energy density spectrum $F(\sigma,\theta,\phi,\lambda,t)$ divided by σ observed in a frame moving with the ocean current velocity, that is, $N(\sigma,\theta,\phi,\lambda,t) = F(\sigma,\theta,\phi,\lambda,t)/\sigma$. The action density is chosen because it is conserved in the presence of time-dependent water depths and currents whereas the energy density spectrum is not., The conservation equation for N in flux form in spherical coordinates and in frequency-direction space is given in the form:

$$\frac{\partial \mathbf{N}}{\partial \mathbf{t}} + (\cos\phi)^{-1}\frac{\partial}{\partial \phi}(\mathbf{c}_\phi \cos\phi \mathbf{N}) + \frac{\partial}{\partial \lambda}(\mathbf{c}_\lambda \mathbf{N}) + \frac{\partial}{\partial \sigma}(\mathbf{c}_\sigma \mathbf{N}) + \frac{\partial}{\partial \theta}(\mathbf{c}_\theta \mathbf{N}) = \frac{\mathbf{S}}{\sigma} \qquad \textbf{(1)}$$

where

$$\mathbf{S = S_{phil} + S_{in} + S_{nl4} + S_{nl3} + S_{ds} + S_{bf} + S_{br}} \quad \textbf{(2)}$$

and $S = S(\sigma,\theta,\phi,\lambda,t)$ is the net source term expressed in terms of energy density, S_{phil} the linear and S_{in} the exponential wave generation mechanisms due to wind, S_{nl4} the quadruplet and S_{nl3} the triad nonlinear wave-wave interactions, S_{ds} the whitecapping dissipation, S_{bf} the dissipation due to bottom friction and S_{br} the wave decay due to depth-induced wave breaking., In Eq. (1) the first term on the left hand side represents the local rate of change of action density in time, the second and third terms the propagation of action density in geographical space (with propagation velocities c_ϕ and c_λ in latitude and longitude space, respectively), the fourth term the shifting of the relative frequency due to variations in depths and currents (with propagation velocity c_σ in σ space) and the fifth term the depth-induced and current-induced refraction (with propagation velocity c_θ in θ space). In wave number space k replaces σ and the velocity c_k in wave number space replaces the velocity c_σ in frequency space. For steady current the absolute frequency $\mathbf{\Omega = \sigma + \vec{k}.\vec{U}_C}$ ($\mathbf{\vec{k}}$ being the wavenumber and $\mathbf{\vec{U}_C}$ the ambient current vectors) is conserved when following the path of a wave group in phase space (Janssen, 2004). For no currents Ω reduces to the intrinsic frequency σ and for time-independent depth σ is conserved. In such conditions $c_k = c_\sigma = 0$, that is, the 4th term on the left hand side vanishes and the depth refraction term (5th term) depends only on the depth gradient. In a Cartesian coordinate system this implies that the action density balance equations in both k- and σ-space reduce to the energy balance equation and that the energy density is also conserved in the absence of energy input for divergent free flow. The energy density, however, is not conserved in the presence of current and unsteady depth.

The term S_{phil} is due to Cavaleri and Malanotte-Rizzoli (1981) but with a filter to eliminate contributions from frequencies lower than the Pierson-Moskowitz frequency

(Tolman, 1992), and is hereafter referred as CR81 while S_{in} is based on the formulations of Komen et al. (1984) and Janssen (1989, 1991). The term S_{nl4} is computed with the discrete interaction approximation (DIA) technique of Hasselmann et al. (1985) which is found to be quite successful, apart from some shortcomings (Krasnopolsky et al., 2002) in capturing the essential features of the wave spectrum (Komen et al., 1994). This source term transfers energy from spectral peaks to lower and higher frequencies in which the energy is redistributed so that there is no net loss or gain of energy due to nonlinear wave-wave interactions. It dominates the evolution of the spectrum in deep and intermediate waters. Two forms of S_{ds} are used in this study, namely, one represented by the quasi-linear model of Hasselmann (1974) and the other by the nonlinear model described in Schneggenburger et al. (2000) while the bottom friction S_{bf} selected is based on the empirical Joint North Sea Wave Project (JONSWAP) model of Hasselmann et al. (1973).

In coastal wave models applied in very shallow water and in inlets and surf zone areas (water depths < 5 m) S_{nl3} and S_{br} are important source terms in the evolution of the spectrum. Under these conditions, and as the surf zone is approached, the processes of depth-induced wave breaking and triad wave-wave interactions may become the dominant processes and cannot be neglected. The formulation of S_{br} is based on Battjes and Janssen (1978) in which shallow water is defined as water depth h = 2 x significant wave height while that of S_{nl3} is based on the lumped-triad approximation of Eldeberky (1996). However, since the models used in this study are not applied in very shallow water and in the surf zone area, the source terms S_{nl3} and S_{br} are generally small and are not activated in the models that contain one or both of them.

b ***WAM4.5***

The WAM was originally developed for open ocean applications and provides reliable data on a global or regional scale down to model grid sizes about two kilometres and water depths above about 5 m. It solves the energy balance form of Eq. (1) for no currents and fixed water depths on a spherical grid and in f-θ space. WAMDI Group (1988) describes the Cycle-3 version of WAM (hereafter referred as WAM3) in which S_{in} and S_{ds} are based on the formulations of Komen et al. (1984). In the WAM4 version, S_{in} and S_{ds} are based on the formulations of Janssen (1989, 1991) in which the winds and waves are coupled. In a two-way coupling there is a feedback of growing waves on the wind profile and of the reduced winds on the growing waves. However, in this study the coupling is one-way, that is, from winds to waves. The effect of this feedback is to enhance the wave growth of younger wind seas over that of older wind seas for the same wind.

WAM4.5 is an update of the WAM4 and incorporates many of the changes described in Monbaliu et al. (2000). It uses the first order upwind explicit propagation scheme which results in the propagation time step being limited by the Courant-Friedrichs-Levy (CFL) condition and a fully implicit source term integration numerical scheme. The latter improvement allows the specification of the source term integration time step to be larger than the propagation time step, thus saving computer time.

The wave generation by wind is described by

$$\mathbf{S_{wnd} = S_{phil} + S_{in}} \qquad \textbf{(3)}$$

where S_{phil} is based on CR81 and is given by

$$\boldsymbol{S_{phil}} = \frac{\mathbf{C_{phil}}}{\mathbf{g^2}} \max[0., \mathbf{u}_* \cos(\boldsymbol{\theta} - \boldsymbol{\theta_{wnd}})]^4 \boldsymbol{H} \qquad \textbf{(4)}$$

with the filter function

$$\mathbf{H = \exp[-(\frac{\sigma}{\sigma^*_{PM}})^4]} \textbf{ and } \mathbf{\sigma^*_{PM} = 2\pi \frac{0.13g}{28u_*}} \qquad \textbf{(5)}$$

θ_{wnd} is the wind direction, u_* the friction velocity, the constant $C_{phil} = 1.5 \times 10^{-3}$ in f-θ space and σ^*_{PM} the peak frequency of the fully developed Pierson-Moskowitz (1964) sea state reformulated in terms of u_*. The main effect of S_{phil} is to improve the somewhat sluggish behaviour of WAM4.5 with respect to wave growth at wind speeds close to zero.

In Eq. (3) the exponential wave growth term

$$\mathbf{S_{in} = \gamma_{in} F(f,\theta)} \qquad \textbf{(6)}$$

where $\gamma_{in} = \gamma_{inJ}$ is the growth rate based on the WAM4 formulation taken from Janssen (1991), that is,

$$\begin{aligned} \gamma_{inJ} &= \frac{1.2}{\kappa^2}\varepsilon\lambda \ln^4 \lambda x^2 \sigma \quad \text{for } \lambda \le 1 \\ &= 0 \qquad\qquad\qquad\quad \text{for } \lambda > 1 \end{aligned} \qquad \textbf{(7)}$$

where ε is the air-water density ratio and

$$x = \max[0., (\frac{u_*}{c} + z_\alpha)\cos(\theta - \theta_{wnd}); \quad \lambda = \frac{g z_0}{c^2}\exp(\frac{\kappa}{x}) \qquad \textbf{(8)}$$

In Eq. (8) c is the phase speed of the wave, $z_\alpha = 0.011$ the shift growth parameter, $\kappa = 0.41$ the von Karman constant and z_0 the surface roughness length given by the Charnock equation

$$z_0 = \alpha_C \frac{u_*^2}{g} \quad \text{and} \quad \alpha_C = \frac{0.011}{\sqrt{1 - \frac{\tau_w}{\tau}}} \qquad \textbf{(9)}$$

where α_C is the sea-state dependent Charnock parameter with τ being the total surface stress and τ_w the wave-induced stress computed by the wave model.

The nonlinear quadruplet (S_{nl4}) and the triad (S_{nl3}) wave-wave interactions both contribute to the evolution of the wave spectrum with the former dominating in deep and intermediate waters and the latter in shallow waters. However, in WAM4.5 only the physics of S_{nl4} are included, the computations of which are carried out by the DIA technique of Hasselmann et al. (1985).

Dissipation is represented in WAM4.5 by whitecapping and bottom friction while that due to depth-induced wave breaking, although included in the model, is not activated for reasons already stated. The Hasselmann (1974) model of S_{ds} is given by

$$\mathbf{S_{ds} = -\gamma_{ds} F(f,\theta)} \qquad \mathbf{(10)}$$

where γ_{ds} is the dissipation rate. Janssen (1991) adjusted γ_{ds} for WAM4 to obtain a proper balance at the high frequencies. Janssen's formulation of γ_{ds} is given by

$$\gamma_{dsJ} = C_{ds}\bar{\sigma}\bar{k}^2 E^2 [(1-\delta)\frac{k}{\bar{k}} + \delta(\frac{k}{\bar{k}})^2] \qquad \mathbf{(11)}$$

in which C_{ds} and δ are tunable coefficients, k the wavenumber, $\bar{k}$ the mean wavenumber, $\bar{\sigma}$ the mean angular frequency and E the total wave variance defined as the integral of $F(f,\theta)$ over all frequencies and directions. In WAM4.5 C_{ds} is taken as 4.5 and δ as 0.5.

The empirical JONSWAP model of the bottom friction is expressed as

$$S_{bf} = -\frac{C_{bf}}{g}\frac{2k}{\sinh(2kd)}F(f,\theta) \qquad \mathbf{(12)}$$

where C_{bf} is also a tunable coefficient whose value is based on the results of the JONSWAP experiment.

To ensure that the WAM remains numerically stable a limitation on wave growth is imposed. This limiter is based on the formulation of Hersbach and Janssen (1999), hereafter referred as HJ99, and gives the maximum total change of energy density per iteration per spectral wave component. It is expressed in f-θ space as

$$|\Delta F(f,\theta)|_{max} = 3.0 \times 10^{-7} g \hat{u}_* f^{-4} f_c \Delta t \qquad \mathbf{(13)}$$

in which f_c is the model prognostic cut-off frequency and Δt *the* source term integration time step. Here $\hat{u}_* = max(u_*, gf^*_{PM}/f)$ *and* $f^*_{PM} = 5.6 \times 10^{-3}$ is the dimensionless Pierson-

Moskowitz frequency. More details of the formulation of the WAM can be found in Komen et al. (1994).

c *SWAN*

SWAN is designed for coastal applications. The physical processes applicable to ocean wave modelling are of coarse also included in coastal wave modelling. Furthermore, additional processes which can be important in coastal systems, e.g., depth-induced wave breaking and triad nonlinear coupling of waves (SWAN, 2004) are also included. SWAN solves the action balance equation on a spherical grid (among other possible grids) and in σ-θ space. The assumptions of time-independent water depths and no currents are also made for SWAN so that the solution of Eq. (1) is equivalent to the solution of the energy balance equation as in the case of WAM4.5. The propagation scheme is fully implicit and for the source term integration scheme the fully implicit option is chosen. The source terms S_{phil}, S_{in}, S_{nl4}, S_{ds} and S_{bf} used in SWAN are basically the same as described for WAM4.5 while S_{nl3} and S_{br} are not activated for the reasons already stated. The coefficient C_{phil} in the source term S_{phil} is calculated as $C_{phil} = 1.5 \times 10^{-3} /(2\pi)$ in σ-θ space. As in WAM4.5 a wave growth limiter is also used in SWAN. This limiter described in Ris (1997), and hereafter referred as R97, is given by

$$|\Delta N(\sigma,\theta)|_{max} = (0.1\alpha_{PM})/(2\sigma k^3 c_g) \quad \textbf{(14)}$$

where $\alpha_{PM} = 0.0081$ is the Phillips constant for a Pierson-Moscowitz (1964) spectrum. Expressed in σ-θ space and in terms of action density the HJ99 limiter Eq. (13) becomes

$$|\Delta N(\sigma,\theta)|_{max} = (2\pi)^2 \times 3.0 \times 10^{-7}\, g\, \hat{u}_* \sigma_c \Delta t/(\sigma^3 k) \quad \textbf{(15)}$$

This limiter is added as an option and is used when the WAM4 option is chosen in SWAN. In the original implementation of SWAN version of WAM4, z_α was omitted in Eq. (8) in the wind input source term S_{in}. The omission of z_α apparently led to underprediction of the significant wave heights as shown in Lalbeharry (2002). Inclusion of this parameter causes a slight enhancement of the normalized growth rate (see Figs. 3.12 and 3.14 in Janssen, 2004) and results in better agreement of the wave heights with those of WAM4.5. More details of the formulation of SWAN can be found in Holthuijsen (2007). The documentation of SWAN version 40.31 used in this study is described in the SWAN (2004).

d ***K-model***

In contrast to SWAN the K-model is a coastal wave model in which the focus is set on limiting the complexity of the modelling approach by retaining only essential physical processes in the wave model for coastal inhomogeneous applications. The K-model is developed in the technical frame of WAM4 for applications in small-scale shallow water environments (Schneggenburger, 1998; Schneggenburger et al., 2000) in which some physical and dynamical properties of WAM4 are retained or modified in the K-model. For example, the numerical implementation of source functions in the K-model is adopted from WAM4. The K-model describes the evolution of the action density $N(k,\theta)$ in k-θ instead of σ-θ coordinate system and uses the same numerical propagation and integration schemes as those of WAM4.5. The assumptions of time-independent depth and no currents are also made for the K-model so that $c_k = c_\sigma = 0$ and Eq. (1) in the k-θ system reduces to the energy balance equation as in the cases of both WAM4.5 and SWAN.

In the K-model only the source functions S_{phil}, S_{in}, S_{ds} and S_{bf} are used. S_{phil} and S_{bf} have essentially the same forms as those in WAM4.5 and SWAN. However, a second filter is applied to S_{phil} which is also rescaled to one-tenth of its original magnitude to reduce the

input for short waves in small-scale applications (Schneggenburger, 1998; Schneggenburger et al., 2000). Expressed in terms of energy density in k-θ space S_{phil} is given as

$$\mathbf{S_{phil} = 0.1 \frac{C_{phil}}{g^2} c_g \max[0., u_* \cos(\theta - \theta_{wnd}]^4 HH_2} \qquad \mathbf{(16)}$$

where the second filter $\mathbf{H_2 = \exp(-\frac{\sigma}{\sigma_{PM}^*})}$ and C_{phil} = 1.5 x $10^{-3}/(2\pi)$.

The source term S_{in} is based on WAM3 in which the Snyder wind input (WAMDI Group, 1988) is modified to include the effect of wind gustiness. The term S_{ds} is a nonlinear dissipation function used as the key dissipation mechanism which accounts for dissipation by wave turbulence interactions. In the K-model Schneggenburger et al. (2000) neglected S_{nl4} and showed that for the coastal wave model the nonlinear dissipation could reproduce qualitative features and empirical laws of wave growth. The equations for S_{in} and S_{ds} as used in the K-model are given by Schneggenburger et al. (2000) as:

$$\mathbf{S_{in} = \beta \sigma G N(k,\theta)} \qquad \mathbf{(17)}$$

in which the gustiness parameter

$$\mathbf{G = \frac{1}{\sqrt{2\pi}} \frac{\sigma_{u_*}}{c_*} \exp[-\frac{(c_* - u_*)^2}{2\sigma_{u_*}^2}] + \frac{1}{2}[\frac{u_*}{c_*} - 1][1 - \Phi(\frac{c_* - u_*}{\sigma_{u_*}})])} \qquad \mathbf{(18)}$$

where

$$\mathbf{c_* = \sigma/[28k\cos(\theta - \theta_{wnd})]; \qquad \Phi(x) = \frac{2}{\sqrt{2\pi}} \int_0^x e^{\frac{-t^2}{2}} dt; \qquad \frac{\sigma_{u_*}}{u_*} = 0.4}$$

(19)

In Eq. (19) $G = 0$ for $\cos(\theta - \theta_{wnd}) < 0$, β = constant, Φ is a probability function and σ_{u_*} is the standard deviation of the assumed normal distribution for the friction velocity. In S_{in} u_* is

replaced by the 10 m level wind speed U_{10} using the fixed relation $28u_* = 1.2U_{10}$ obtained by tuning the peak frequency of the deep-water fully developed spectrum.

The nonlinear dissipation function is given by

$$\mathbf{S_{ds} = -\gamma_K g k^5 [\coth(2kd) + \frac{kd}{\sinh^2(kd)}] N^2(k,\theta))} \quad \textbf{(20)}$$

with

$$\gamma_K(N) = \gamma_0 \frac{p_1 (p_2 \frac{k}{\bar{k}})^q + 1}{(p_2 \frac{k}{\bar{k}})^q + 1} \quad \textbf{(21)}$$

The required parameters in S_{in} and S_{ds} are prescribed according to those used for the North Sea application in Schneggenburger (1998). For S_{in} $\beta = 0.006$ and for S_{ds} $\gamma_0 = 0.06775$, $p_1 = 4$, $p_2 = 1.2$ and $q = 8$. The K-model adopts the HJ99 limiter expressed in the k-θ coordinate system and its source functions S_{in} and S_{ds} are, respectively, different from those implemented in WAM4.5 and SWAN. Table 1 summarizes the source term, growth limiter and depth refraction options applied to each of the three models.

e *Model Implementation*

All models are run on the same grid with a spatial resolution of $\Delta\lambda = \Delta\varphi = 0.05°$. The maximum dimensions of Lake Erie are about 400 km in length and 100 km breadthwise and the water depths ranges from 5 – 60 m. This lake can, therefore, be considered shallow enough to be used as a candidate for testing the models in shallow water depth or transitional water depth mode. In this study the WMO (1998) definitions of deep water, transitional depth and shallow water characterized by the ratio between water depth and wavelength are applied. A significant area of Lake Erie has water depths h < 25 m. A peak period of 8 s gives

a deep water wavelength L = 100 m. As shown later in this study peak periods ~ 8 s were observed in Lake Erie, in which case L/25 < h < L/4 characterizes transitional water depths (WMO, 1998).

The three models were initialized to run in shallow water mode with depth refraction on the spherical model grid for Lake Erie. It is assumed that there are no currents and that the water depths are time-independent. The solution of Eq. (1) is provided for 24 directional bands at 15° each with the first direction being 7.5° measured clockwise with respect to true north and 25 frequencies logarithmically spaced from 0.05 Hz to 0.49 Hz at intervals of $\Delta f/f = 0.1$. In the case of the K-model there are 25 wavenumbers also logarithmically spaced from 0.01 m^{-1} to 0.97 m^{-1} at intervals of $\Delta k/k = 0.21$. In finite water depth $(L/25 < h < L/4)$ the wave energy propagates with the group velocity $c_g = c/2[1 + 2kh/\sinh(kh)]$ where $c = [g/k)\tanh(kh)]^{1/2}$ is the phase speed, For deep water (h > L/4) $c_g = c/2$, $c = g/(2\pi f)$ and $L = 1.56T^2$ m where T is the wave period in seconds. For shallow water $(h < L/25)$ $c_g = c = (gh)^{1/2}$ in which both the group and phase velocities are functions only of the water depth. As the waves move from deep to intermediate and shallow waters, the wave height increases due to shoaling but after this initial rise the height decreases as wave energy is lost to bottom friction. The shallow water physics include only the bottom friction source term based on the formulation of Hasselmann et al. (1973). The dissipation constant C_{bf} in Eq. (12) is set to $0.01\ m^2s^{-3}$ in the K-model corresponding to the parameters set in S_{in} and S_{ds} (Schneggenburger et al., 2000) and to the JONSWAP value $0.038\ m^2s^{-3}$ in both WAM4.5 and SWAN. Test runs using $C_{bf} = 0.067\ m^2s^{-3}$ for windsea conditions in WAM4.5 and SWAN indicate minimal differences (not shown) when the results are compared against those using $C_{bf} = 0.038\ m^2s^{-3}$ for swell conditions. The depth-induced wave breaking option is deactivated in both WAM4.5 and SWAN while the triad option is deactivated in the latter only as this source term is not included in the former. The propagation and integration time

steps which take into consideration the CFL criterion and the CPU times used by each of the three models are shown in Table 2. It is seen that WAM4.5 consumes far less CPU time than the other two models for the same run, which may indicate that WAM4.5 is more optimized than both SWAN and the K-model.

Fig. 1 shows the computational domain and the bathymetry for Lake Erie with water depths ranging from 5 m to 60 m and the locations of the buoys used in the verification of the model results. It is seen that a significant area of Lake Erie lies in water depths < 25 m. The buoys are located in water depth of 14.5 metres (45005), 22 metres (45132) and 27 metres (45142). Given a deep water wave peak period of 8 s, buoys 45005 and 45132 are located in intermediate water depth while buoy 45142 is considered to be in deep water.

The three wave models are run in a hindcast mode for the three-week period 12 November – 4 December 2003. The period is chosen because it includes a remarkable storm event which generated high wind speeds and significant wave heights at 1500 UTC on the 13 November in the north-eastern part of the lake. For the hindcast runs the wave models use the same inputs, namely, a time-independent bathymetry for Lake Erie and the 3-hourly 10 m level driving wind fields. The wind dataset is created by assembling the 0, 3, 6 and 9 forecast hour winds of the 0000 and 1200 UTC daily runs of the Canadian Meteorological Centre (CMC) weather prediction model to produce a quasi-hindcast wind dataset for the time period of this study since the analysed winds valid, respectively, at 0300, 0600, 0900, 1500, 1800 and 2100 UTC are not available. The 00-h forecast wind field approximates the analysed wind field valid at run time 0000 UTC or 1200 UTC except for initialization and interpolation procedures and gravity waves filtering. The 3-, 6- and 9-h winds are actually forecast winds obtained from the CMC weather prediction model 0000 UTC or 1200 UTC run. Because of small model errors, it is reasonable to assume that the 3-, 6- and 9-h forecast winds from the 0000 UTC run is a close approximation to the analysed wind fields valid,

respectively, at 0300, 0600 and 0900 UTC and those from the 1200 UTC run at 1500, 1800 and 2100 UTC. Each wave model is spun up for two days (from 0000 UTC 10 – 0000 UTC 12 November) prior to the start of the wave simulation runs to ensure that the initial wave fields are realistic for the start of the hindcast period at 0000 UTC 12 November. The results obtained by each of the three different wave models in shallow water mode with depth refraction and without tidal influences are compared with observations at the three buoy locations shown in Fig. 1.

3. Results and discussions

a. *Time series of integrated wave and wind parameters*

During the chosen three week hindcast period unusual wave conditions were observed in Lake Erie. Snapshots in Fig. 2 show the distributions of (a) WAM4.5 significant wave height (SWH), (b) WAM4.5 peak period (T_p), (c) K-model SWH and (d) SWAN SWH valid 1500 UTC 13 November 2003. The corresponding wind field common to the three models is superimposed on the SWH field in Fig. 2a. At that time north-westerly winds are prevailing with wind speeds reaching about 25 ms^{-1} and model-generated SWH reaching 6 m or more in the northeastern part of the lake. The model wave conditions shown at the three buoy locations shown in Fig. 2a are also remarkable, especially taking into account that wind fetch and duration for the development of the waves at these locations are relatively short. The peak period in Fig. 2b is less than 10 s, which corresponds to model waves being mostly windsea. The three models generate peak SWH up to 6 m or more mainly in the same location although the area enclosed by the 6 m contour varies from one model to the other.

Time series plots of measured and computed significant wave height, peak period, wind speed and wind direction at buoy location 45132 are presented in Fig. 3a, those at buoy location 45142 in Fig. 3b and those at buoy location 45005 in Fig. 3c. For buoy 45142 wave

observations are valid up to 0000 UTC 22 November and wind observations up to 1200 UTC 26 November, after which the observations are not valid because of instrument malfunction or the buoy ceases to make observations. The comparison between the observed winds and those obtained by the CMC weather prediction model at these three locations provides the proof that the computed wind fields are of excellent quality. During the major wave episode of 1500 UTC 13 November the observed wind speed varies from 20 to 21 ms^{-1} while that of the model varies from 22 to 24 ms^{-1} as substantiated also in Fig. 2a. The wind statistics discussed in in Section 3c further confirm the quality of the model winds. This is a very good precondition for the calculation of the waves which depend on the quality of the driving wind force.

At the buoy 45132 located in water depth of 22 m , three main episodes of high wind speeds can be detected on the 13, 25 and 30 November, with the most pronounced one at 1500 UTC 13 November (Fig. 3a(iii)). These events are associated with the highest waves and longest peak periods included in the time series as shown in the upper two panels. The agreement between the measurements and the results of all three wave models are very good for the significant wave heights. The measured peaks in the three abovementioned episodes are only slightly overestimated by the wave models. The biggest difference of about 1.2 m occurs at the first and highest peak at 1500 UTC 13 November between the values recorded by the buoy and those obtained by WAM4.5. This overprediction of the wave height is also reflected in the overprediction of the wind speed at that time as shown in Fig. 3a(iii). The results of SWAN and the K-model are closer to the measurements for this special peak. In contrast to the wave height comparisons, Fig. 3a(ii) indicates WAM4.5 performs better than SWAN and the K-model for the peak periods. These time series show a slight underestimation of the observed peak periods by WAM4.5 and SWAN and a more pronounced underestimation by the K-model. The same is also true for the model mean

periods for the no-current case in Schneggenburger et al. (2000) when compared against floater measurements.

In Fig. 3b at the buoy 45142 which is located in water depth of 27 m in the northeast section of the lake (Fig. 1), the model results are quite similar to those obtained at buoy 45132 during the period of observations at buoy 45142. It is interesting to note that the WAM4.5 peak SWH of 5 m agrees exactly with the observed value and lies in the area enclosed by the 5 m contour in Fig. 2a. This lends credence to the model generated wave height of 6 m or more in the vicinity of this buoy as shown in Fig. 2. The WAM 4.5 T_p close to 9 s agrees reasonably well with the observed T_p of 10 s.

Fig. 3c displays the same time series plots as in Fig. 3a but at buoy 45005 located in water depth of 14 m. The major wave episode also occurs here at 1500 UTC 13 November with the observed peak SWH being 3 m. Both WAM4.5 and the K-model overestimate this peak by about 1.0 m in response to the slight overprediction of the wind speed as seen in Fig. 3c(iii). However, SWAN peak SWH, although overestimated, is in better agreement with the observed peak. The WAM4.5 SWH and the K-model SWH are in close agreement throughout the simulation period. The same is also true for their corresponding peak periods. This result seems to suggest that in the approach to shallower waters as in the case of buoy 45005 the nonlinear S_{ds} source term tends to somewhat compensate for the absence of the S_{nl4} source term of the K-model and hence makes the latter comparable to WAM4.5.

b. *One-dimensional and two dimensional spectral analysis*

The foregoing results apply to integrated wave parameters of significant wave height and peak period. We now turn to a comparison of one-dimensional spectra for further insight into the comparative performance of the three models. Accordingly, time series plots of buoy and model one-dimensional (1-D) spectra (m^2Hz^{-1}) at 3-hourly intervals in which the energy

densities are contoured in terms of colour scales are presented in Fig. 4 at buoy location 45132 and in Fig. 5 at buoy location 45005. This kind of data treatment enables a good survey of the development of the spectra in time at both locations. The identification of the three main wave height episodes at buoy 45132 detected already in the corresponding time series for the integrated parameters is very easy because exactly around these peak times the energy densities reach their respective maximum values above 10 m^2Hz^{-1} (yellow and blue areas) at about 0.12 – 0.14 Hz for the buoy in Fig. 4a. In comparison with the buoy spectra the time series of the spectra obtained by the different wave models behave fairly well in shape and time flow whereas there is a little more energy at the peaks in WAM4.5 than in the K-model and SWAN. Furthermore, the area of maximum energy density in the K-model in Fig. 4d is shifted a little bit to higher frequencies centred around 0.16 Hz supporting the fact that the K-model underestimates the peak periods in this application. The time series plots in Fig. 5a at the buoy location 45005 located in water depth of 14 metres show mainly two episodes of high energy densities near 9 m^2Hz^{-1} (green areas) although the general trend is similar to that in the time series for buoy 45132. The high energy densities at the first peak recorded at the buoy are slightly overestimated by WAM4.5 whereas the K-model and SWAN compute smaller values which match better with the measurements in this case. The buoy energy densities for the second peak on the 25 November 2003 are in good agreement with those obtained by WAM4.5 and the K-model. In the SWAN simulation of this peak the corresponding energy density is somewhat weaker.

A closer examination of Figs. 4 and 5 indicates that in the case of the major wave episode near 1500 UTC 13 November the peak frequencies in the K-model are higher than the corresponding peak frequencies generated by WAM4.5 and SWAN. The same is also true for the third wave episode at buoy 45132 around 1200 UTC 30 November. Now, the S_{nl4} source term does not change the total energy of the spectrum (note the good agreement of the

K-model wave heights with those of WAM4.5 in Figs. 3a(i), 3b(i) and 3c(i)). Rather, it redistributes the energy from the peak frequency to lower frequencies and partially to higher frequencies. This redistribution of energy by S_{nl4} is more applicable in deep and intermediate waters. This source term is absent in the K-model but present in both WAM4.5 and SWAN. The better agreement of the WAM4.5 and SWAN peak periods with observations (see Figs. 3a(ii) and 3b(ii)) seems to suggest the importance of the S_{nl4} source term in energy redistribution to provide more accurate model peak periods for more homogeneous systems in which there is an absence of tides and currents. It should be noted also that in Schneggenburger et al. (2000) the K-model mean periods are also underpredicted when compared against floater measurements. One may conclude that for water depths above about 5 m and for homogeneous systems, as in the case of Lake Erie, the source term S_{nl4} should not be neglected in coastal wave models. Similarly, for water depths below about 5 m and for nonhomogeneous applications the source terms S_{nl3} and S_{br} should be included in coastal wave models as shown in Moghimi et al. (2005).

The buoys used for verification provide no two-dimensional (2-D) spectra, but in spite of that it is worthwhile to compare the 2-D spectra of the three wave models as presented in Fig. 6 for the most pronounced event at 1500 UTC on 13 November 2003 at buoy location 45132. The different models show quite similar 2-D spectral patterns with the individual wave direction at the model peak close to the wind direction. However, peak intensities and peak locations in frequency range vary from one model to the other with WAM4.5 peak being the most intense (near 16 m^2 Hz^{-1} rad^{-1}; blue area) and SWAN peak being the weakest (near 16 m^2 Hz^{-1} rad^{-1}; pink area). These differences are reflected in the comparisons between measured and computed time series of integrated parameters and 1-D spectra at this location at the time of the 2-D spectra, that is, the overprediction of the wave heights in WAM4.5 and K-model runs and the underprediction of the peak period by the K-model. In Fig. 6 the

frequency of the peak 2-D energy for the K-model is somewhat higher than those corresponding, respectively, to the peak 2-D energies of WAM4.5 and SWAN. Even though the 2-D spectral energy density for each of the three models is valid for one snapshot time, it lends support to the discussion on the time series plots of the 1-D spectra in Figs. 4 and 5.

c. Validation statistics

Fig. 7 presents scatter plots of model versus buoy significant wave heights >= 0.1 m and peak periods >= 2.0 s for the period 12 November – 4 December 2003. The plots are based on the available observations at buoys 45132, 45005 and 45142. The plots indicate that a maximum value close to 5 m is observed by the buoy and simulated by WAM4.5 while SWAN and the K-model generated a value close to 4 m. The observed value near 5 m appears in the time series plots of the wave heights in Fig. 3b(i) at buoy location 45142.

The scatter plots complement the validation statistics described below and provide a more appealing way of displaying the same information. A very good quantification of the model performances is provided by the symmetric slope, s, defined in the Appendix and shown as the red solid lines in the scatter plots in Fig. 7. It is the regression coefficient of the line constrained to pass through the origin obtained by fitting data pairs of model and observed values (Bauer et al., 1992). It gives a measure of the deviation of the data pairs from the perfect fit straight line. The trend for the wave heights (Figs. 7a to 7c) and the peak periods (Figs. 7d to7f) becomes apparent by directly looking at the relation between the black lines which denote the perfect fit to model and observed values and the red symmetric slope lines. Figs. 7a and 7c show slight overprediction of the observed significant wave heights by WAM4.5 and the K-model whereas the lines in Fig. 7b are very close together for SWAN. The scatter plots in Figs. 7d and 7e show slight underprediction of the peak periods by WAM4.5 and SWAN. An important conclusion of the study by Soomere et al. (2008)

corroborated one of the basic outcomes of our study that WAM4.5 tends to overpredict wave heights and underpredict wave periods in strong storms in intermediate-scale water bodies. However, in the case of the K-model the underprediction is more pronounced as seen in Fig. 7f especially for larger periods. This may be ascribed to the absence of the quadruplet nonlinear wave-wave interactions in the K-model as applied in Lake Erie.

The buoy data provide an independent data set to objectively evaluate the accuracy and quality of the model wave parameters. Table 3 gives the validation statistics for the significant wave heights, Table 4 those for the wave periods and Table 5 those for the wind speeds. The three tables represent the results of the statistical analysis of the comparisons between the buoy measurements and the wave and wind data of each of the three wave models. From the definition of bias (see the Appendix) negative values denote underprediction and positive values overprediction. In the computations of anomaly correlation coefficient, ac, and the reduction of variance, rv, the buoy mean of all the observations is used as climatology. Both ac and rv are skill scores since they provide a measure of how much more skill the model wave parameter has over the unskilled estimate based on climatology which is the buoy mean value in this case. In the wave modelling community a wave forecast or hindcast is considered to be useful if the anomaly correlation is above 0.6 (Janssen et al., 1997), which is definitely the case for all three models with values around 0.9 for the wave height comparisons and about 0.7 – 0.8 for the peak periods.

The skill value of rv should be between 0 and 1 in which 1 is the ideal value denoting that measurements and wave model results are the same. Values below 0 indicate that a climate mean of the observations is better than the wave model results. The reduction of variance in Table 3 for the significant wave heights varies between 0.764 and 0.879 and proves that all wave models actually provide wave heights of excellent quality. The values for rv in Table 4 for the peak periods are 0.717 for WAM4.5 and 0.716 for SWAN but only

0.409 for the K-model. This shows that the K-model has definitely problems to calculate satisfactory peak periods in an application on an intermediate scale. As discussed earlier this shortcoming of the K-model is related to the exclusion of the S_{nl4} source term. This is also supported by the bias for the K-model of -0.583 which is much higher than those of WAM4.5 (-0.112) and SWAN (-0.150). The values for s are included in Table 3 (wave heights) and Table 4 (peak periods). The scatter index SI is another skill index. The objective of ocean wave modellers is to achieve an SI of the order of 15% or less (Jensen et al., 2006; Cardone et al., 1995). The K-model shows less skill than the other two models and suggests that wave model development has not reached its limit in response to the rhetorical question posed by Liu et al. (2002). Except for the K-model peak periods the validation statistics summarised in Tables 3 and 4 give further proof that the wave models agree fairly well with the observations during the three weeks hindcast for Lake Erie.

In the study by Liu et al. (2002) the time series comparisons of the four models reflect the general trend and patterns of the wave measurements but they do show some disagreement with each other. Since wind input, numerics and resolution are assumed to be adequate, the deviations from the measurements suggest remaining deficiencies of wave model physics. In the analysis the mean correlation coefficient for dominant wave period between model and measurement is higher for the WAM4 (80%) than those (58 – 72%) corresponding to the other three models with different physics. In our opinion the notion that wave model development may have reached its limit is somewhat pessimistic since there is still scope to have further refinements of the physics to improve the match between model results and measurements. In our study the correlation coefficients for wave heights given in Table 3 for WAM4.5, SWAN and the K-Model range from 91 – 94 % indicating some improvement in wave model development.

In Table 5 the wind speed statistics indicate the weather prediction model shows skill in that ac > 0.9 and rv > 0.7. However, further improvement in wind accuracy is needed to reduce the SI below 25% although this is not too an unreasonable value for intermediate scale application such as Lake Erie. The bias is positive, that is, wind speeds tend to be overpredicted as seen also in Figs. 3a(iii), 3b(iii) and 3c(iii), respectively. For a fully developed sea it can be shown that $\delta H_s/H_s = 2\delta U_{10}/U_{10}$. For a 10% error in U_{10}, $\delta H_s/H_s$ = 0.2 so that for an H_s of 5 m as generated by the WAM4.5, this error in wind speed is likely to produce an error in H_s ~ 1.0 m. The standard deviation of error of H_s in Table 3 is about 0.3 m, which is well below the 1 m produced by 10% error in wind speed for the Lake Erie case.

4 Summary and conclusions

Three state-of-the-art wave models, namely the ocean model WAM4.5 and the two coastal models SWAN and the K-model are used in this investigation in a hindcast mode to generate waves in Lake Erie. The objective of the study is to determine which approach is the appropriate one to provide the best possible wave data in an application on an intermediate scale taking into consideration the relative performances of the three models in an enclosed water basin such as Lake Erie.

The wave models are applied in shallow water mode with depth refraction and bottom friction and without tidal influences for the three-week time period 12 November – 4 December 2003. The results obtained by each of the models are validated against observations at three buoy locations. Time series plots of measured and computed integrated parameters, one-dimensional spectra and a detailed statistical analysis indicate that the three wave models perform reasonably well in simulating the wave parameters. The model results are quite comparable especially for the significant wave heights which are slightly

overpredicted by the models. The observed peak periods are slightly underestimated by WAM4.5 and SWAN but the underestimation is more noticeable in the K-model. Since the quadruplet non-linear wave interaction term is largely responsible for transfers of wave energy to lower frequency waves, this supports the conclusion that this term should not be neglected.

Comparing the performances of the three models in this study, WAM4.5 seems to be a reasonable choice for use in an operational environment instead of the coastal wave models SWAN and K-model in an application on such intermediate scale as Lake Erie. Our study shows that the K-model is already near its limit in this application as the spatial resolution seems to be too coarse. This model is more applicable for smaller scale inhomogeneous systems in a coastal environment with tidal influence (Schneggenburger et al., 2000; Schneggenburger, 1998). As the systems become larger in scale and less variable, the applicability of the K-model is diminished because nonlinear transfer of energy, which is neglected in the K-model, becomes an important source term in these systems. For application to coastal wave modelling, SWAN is more a suitable candidate for nesting with WAM4.5. In this study SWAN demonstrates a better performance than the K-model. Addtionally, both WAM4.5 and SWAN have (f, θ) spectral coordinates as opposed to the spectral (k, θ) coordinates of the K-model and would avoid the problem associated with the transformation of the boundary spectra from the (f, θ) axes of WAM4.5 to the (k, θ) axes of the K-model.

Appendix. Description of statistical parameters

bias = $1/n\Sigma(Y_i - X_i)$ **is the mean error.**

stddev = $[1/N\Sigma(Y_i - X_i - Bias)^2]^{1/2}$ **the standard deviation of errors.**

SI = stddev/(Buoy Mean) **the scatter index.**

$r = [1/N\Sigma(Y_i - Y_{mean})(X_i - X_{mean})]/\sigma_y\sigma_x$ **the linear correlation coefficient.**

$ac = \sum(Y_i - X_c)(X_i - X_c)/[\sum(Y_i - X_c)^2(X_i - X_c)^2]^{1/2}$ **the anomaly correlation.**

$rv = 1 - \sum(Y_i - X_i)^2/\sum(X_i - X_c)^2$ **the reduction of variance.**

$s = [\sum Y_i^2/\Sigma X_i^2]^{1/2}$ **the symmetric slope.**

Here, X_i and Y_i are, respectively, the i^{th} observed and model values, X_c the climatology of X defined here as the mean of the total buoy observations, σ_y the standard deviation of Y, σ_x that of X and N the number of observations.

References

Battjes, J. A. and J. P. F. M. Janssen, 1978. Energy loss and set-up due to breaking of random waves. Proc. 16th Conf. Coastal Engineering (Hamburg), New York, ASCE, 569-587.

Bauer, Eva, Susanne Hasselmann and Klaus Hasselmann, 1992. Validation and assimilation of Seasat altimeter wave heights using the WAM wave model. J. Geophys. Res., 98C, 12671-12692.

Booij, N., R. C. Ris and L. H. Holthuijsen, 1999. A third generation wave model for coastal regions 1. Model description and validation. J. Geophy. Res., 104, C4, 7649-7666.

Cavaleri, L. and P. Malanotte-Rizzoli, 1981. Wind wave prediction in shallow water: Theory and applications. J. Geophys. Res., 86, 10961-10973.

Cardone, V. J., H. C. Graber, R. E. Jensen, S. Hasselmann and M. J. Caruso, 1995. In search of the true surface wind field in SWADE IOP-1: Ocean wave modeling perspective. The Global and Atmosphere and Ocean System, Vol. 3(2-3), 107-150.

Donelan, M.A., 1977. A simple numerical model for wave and wind stress prediction. National Water Research Institute manuscript, Burlington, Ontario, Canada, 28 pp

Eldeberky, Y. 1996. Nonlinear transformation of wave spectra in the nearshore zone. Ph.D. thesis, Delft University of Technology, Department of Civil Engineering, The Netherlands.

Hasselmann, K., 1974. On the spectral dissipation of ocean waves due to whitecapping. Boundary-Layer Meteorol., 6, 107-127.

Hasselmann, K., T. P. Barnett, K. Bouws, H. Carlson, D. E. Cartwright, K. Enke, J. I. Ewing, H. Gienapp, D. E. Hasselmann, P. Kruseman, A. Meerburg, P. Muller, K. Richter, D. J. Olbers, W. Sell and H. Walden (1973). Measurements of wind-wave growth and swell decay during the Joint North Sea Wave Project (JONSWAP), Dtsch. Hydrogr. Z. Suppl., 12, A8, 95p.

Hasselmann, S., K. Hasselmann, J. H. Allender and T. P. Barnett,1985. Computations and parameterizations of the nonlinear energy transfer in a gravity-wave spectrum. Part II: Parameterizations of the nonlinear transfer for application in wave models. J. Phys. Oceanogr., 19, 745-754.

Hersbach, H. and P. A .E. M. Janssen, 1999. Improvement of the short-term behaviour in the wave ocean model (WAM). J. Atmos. Oceanic Techn., 16, 884-892.

Holthuijsen, Leo H., 2007: Waves in Oceanic and Coastal Waters. Cambridge University Press, Cambridge, 387p.

Hughes, S.A., Jensen, R.E., 1986. A User's Guide to SHALWV: Numerical Model for Simulation of Shallow-Water Wave Growth, Propagation, and Decay, Instruction Report CERC–86–2. US ArmyCorps of Engineer Waterways Experiment Station.

Janssen, Peter, 2004. The interaction of the ocean waves and wind. Cambridge University Press, pp 116-128.

Janssen, P. A. E. M., B. Hansen, and J. R. Bidlot (1997). Verification of the ECMWF wave forecasting system against buoy and altimeter data. Wea. Forecasting, 12, 763-784.

Janssen, P. A. E. M., 1989. Wave-induced stress and the drag of air flow over sea waves J. Phys. Oceanogr., 19, 745-754.

Janssen, P. A. E. M., 1991. Quasi-linear theory of wind-wave generation applied to wave forecasting. J. Phys. Oceanogr., 21, 1631-1642.

Jensen, R. E., V. J. Cardone and A. T. Cox, 2006. Performance of third generation wave models in extreme hurricanes. Proc. 9th Int. Workshop on Wave Hindcasting and Forecasting, Victoria, British Columbia, Canada, 24-29 September 2006. Available on CD from Environment Canada.

Komen, G. J., L. Cavaleri, M. Donelan, K. Hasselmann, S. Hasselmann, and P. A .E. M. Janssen, 1994. Dynamics and Modelling of Ocean Waves, Cambridge University Press, Cambridge, 532p.

Komen, G. J., S. Hasselmann and K. Hasselmann, 1984. On the existence of a fully developed windsea spectrum. J. Phys. Oceanogr., 14, 1271-1285.

Krasnopolsky, V. M., D. V. Chalikov, and H. L. Tolman, 2002: A neural network technique to improve computational efficiency of numerical oceanic models. Ocean Modelling, v. 4, 363-383.

Lalbeharry, R., 2002. Comparison of the performances of three state-of-the-art ocean wave models in extreme storm cases. Proc. 7th Int. Workshop on Wave Hindcasting and Forecasting, Banff, Alberta, October 21-25, 2002. Published by Environment Canada.

----------, W. Luo and L. Wilson, 2001. A shallow water intercomparison of wave models on Lake Erie. Proc. 4th Int. Symp. on WAVES 2001, 2-6 September 2001, San Francisco, California, U.S.A. B. L. Edge and J. M. Hemsley (Eds), Am. Soc. Civ. Eng., pp. 550-559.

Lin W, L. P. Sanford and S. E. Suttles, 2002. Wave measurement and modeling in Chesapeake Bay. Cont Shelf Res 22:2673–2686

Lin, W., 2000. Modeling surface wind waves and their effects on air-sea fluxes in Chesapeake Bay. Ph.D. dissertation, University of Maryland Center for Environmental Science, Cambridge, MD, 226 pp.

Liu, Paul C., David J. Schwab and Robert E. Jensen, 2002. Has wind-wave modeling reached its limit? Ocean Eng., 29, 81-98.

Moghimi, Saeed, Gerhard Geyer, Heinz Guenther and Mehdi Shafieefar, 2005. Application of third generation shallow water wave models in a tidal environment. Ocean Dynamics, 55, 10-27.

Monbaliu, Jaak, Roberto Padilla-Hernandez, Julia C. Hargreaves, Juan Carlos Albiach, Weimin Luo, Mauro Sclavo and Heinz Guenther, 2000. The spectral wave model, WAM, adapted for applications with high resolution. Coastal Eng., 41, 41-62.

Pierson, W. J. and L. Moskowitz, 1964. A proposed spectral form for the fully developed wind seas based on the similarity theory of Kitaigorodskii. J. Geophys. Res., 69, 5181-5190.

Resio, D.T., 1981. The estimation of wind–wave generation in a discrete spectral model. J. Phys. Oceangr. 11, 510–525.

Ris, R. C., L. H. Holthuijsen and N. Booij, 1999. A third generation wave model for coastal regions 2. Verification. J. Geophy. Res., 104, C4, 7667-7681.

Ris, R. C., 1997. Spectral modelling of wind waves in coastal areas. PhD Thesis, Delft University of Technology, Delft, Netherlands.

Schneggenburger, C., 1998. Spectral wave modelling with nonlinear dissipation. PhD. Thesis, University of Hamburg, GKSS External Report, 98/E/42.

Schneggenburger, C., H. Guenther and Wolfgang Rosenthal, 2000. Spectral wave modelling with non-linear dissipation: validation and applications in a coastal tidal environment. Coastal Engineering, 41, 201,235.

SWAN (2004) User Manual SWAN Cycle III version 40.31, February 5, 2004. Delft University of Technology, Department of Civil Engineering, the Netherlands.

Soomere, T., A. Behrens, L. Tuomi, and J. W. Nielsen, 2008. Wave conditions in the Baltic Proper and in the Gulf of Finland during windstorm Gudrun. Natural Hazards and Earth System Sciences 8, 1, 37– 46.

Soomere, Tarmo, 2005. Wind wave statistics in Tallinn Bay: Boreal Environmental Research, 10, 103-118.

Tolman, H. J., 1992. Effects of numerics on the physics in a third generation wind-wave model. J. Phys. Oceanogr., 22, 1095-1111.

WAMDI Group, 1988. The WAM model - A third generation ocean wave prediction model. J. Phys. Oceanogr., 18, 1775-1810.

World Meteorological Organization, 1998. Guide to Wave Analysis and Forecasting, WMO-No. 702, 2nd ed., 159 pp.

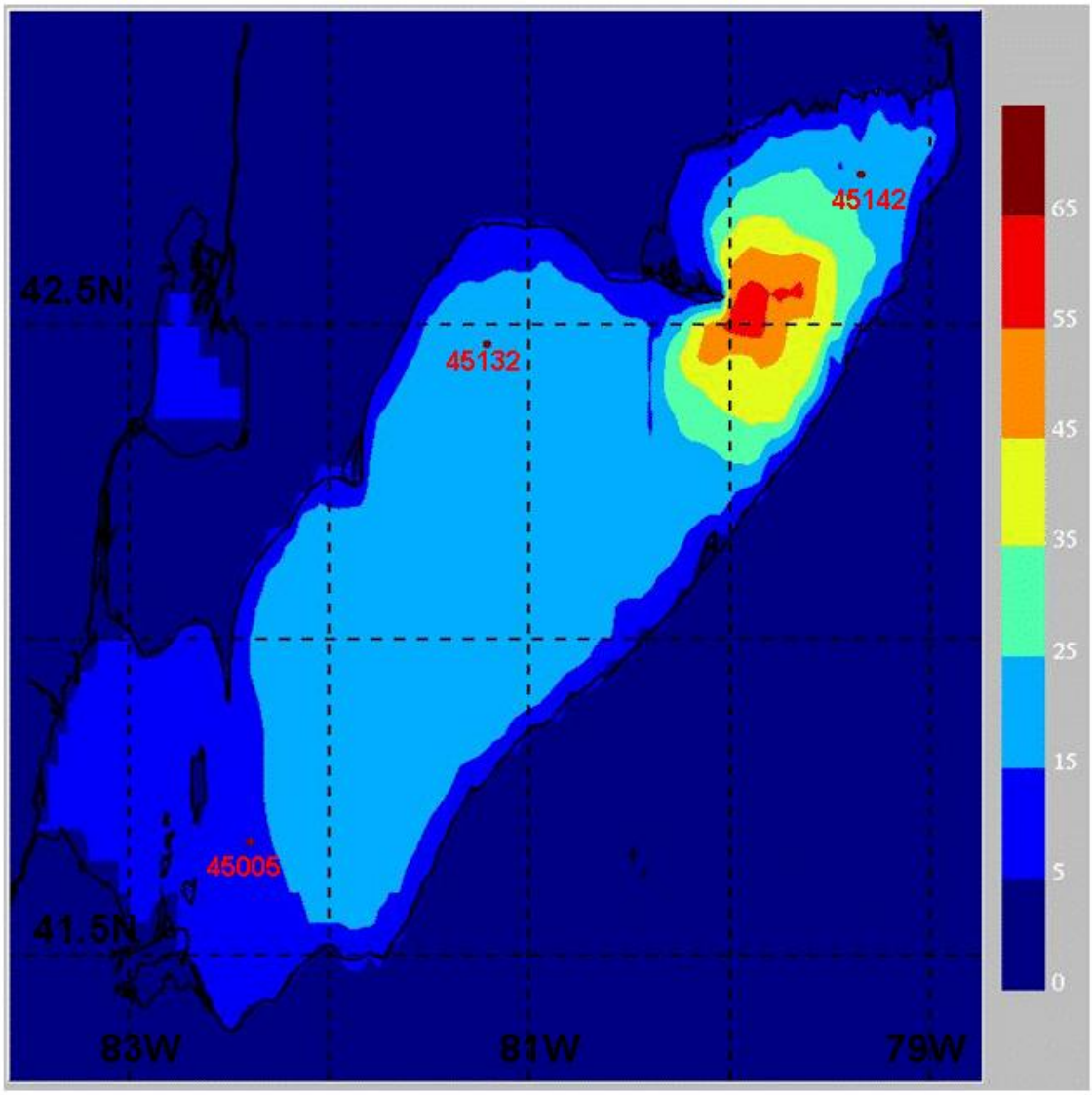

Fig. 1 Lake Erie bathymetry in metres and locations of buoys 45005, 45132 and 45142 used in the verification of model results.

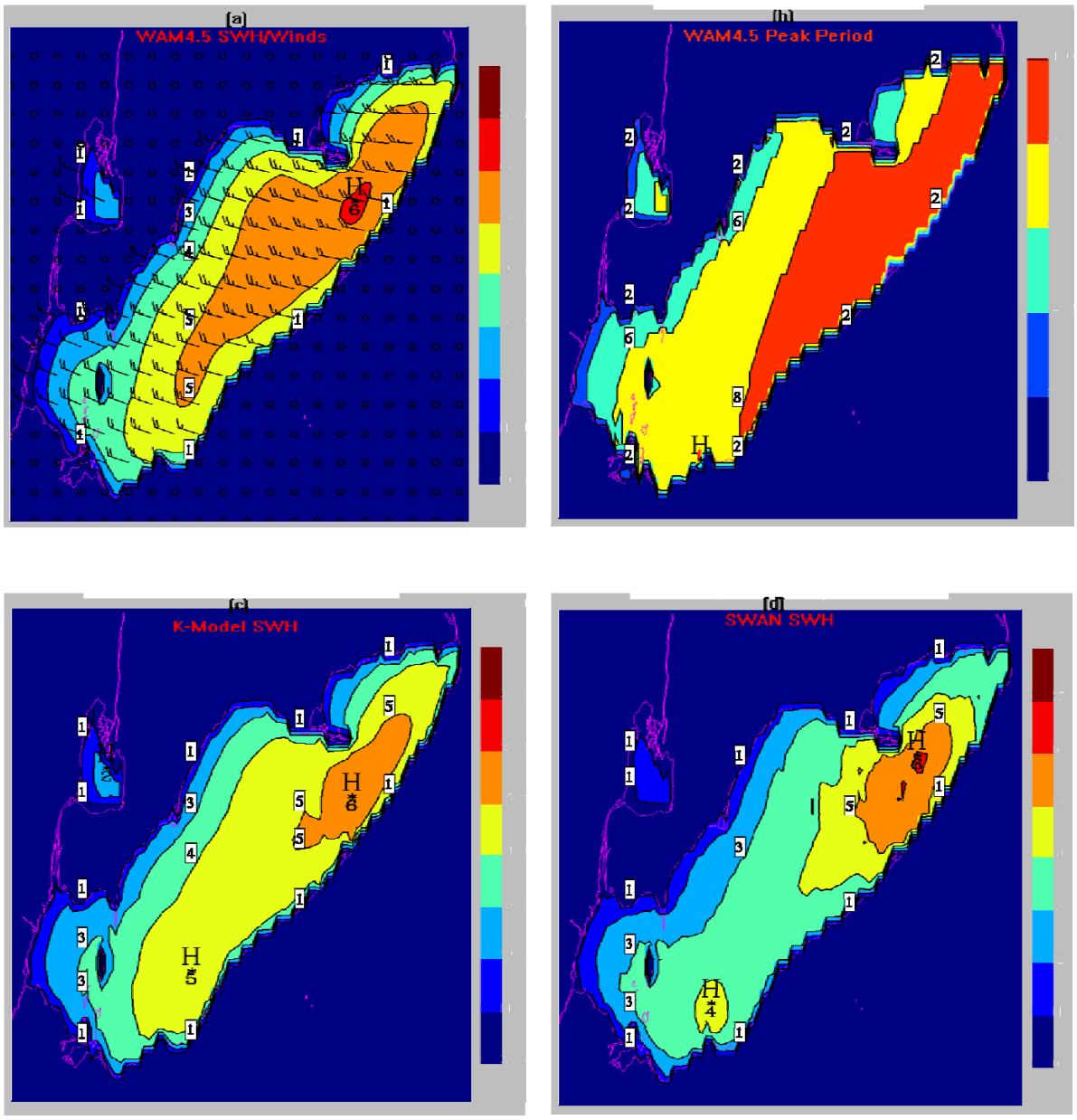

Fig. 2 Snapshots of (a) WAM4.5 SWH, (b) WAM4.5 peak period, (c) K-model SWH and (d) SWAN SWH valid 1500 UTC 13 November 2003. The corresponding wind field input to the three models is superimposed on (a). The wave height contours are given in metres and the winds in meteorological convention with full barb indicating 10 ms^{-1} and half-barb as 5 ms^{-1}. In the figure H indicates the maximum central value.

(a)

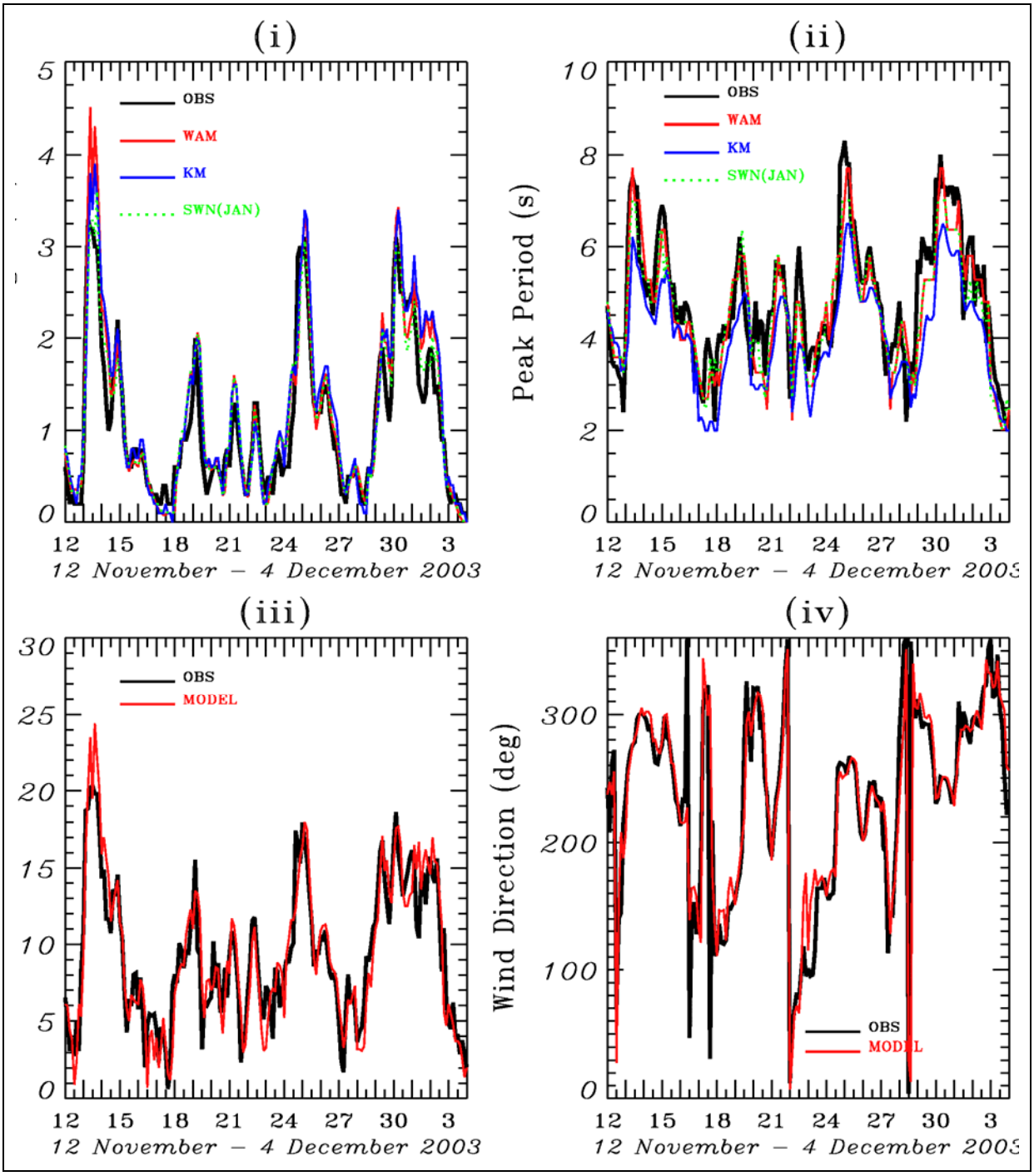

Fig. 3 (a) Time series of observed and modelled (i) significant wave heights (SWH), (ii) peak wave periods, (iii) wind speeds and (iv) wind directions at buoy location 45132 for the time period 12 November - 4 December 2003. In the figure legend "SWN(JAN)" denotes the SWAN option of Janssen's WAM4 as modified in this study and "MODEL" refers to WAM4.5, SWAN or the K-Model . (b) As in Fig. 3a but for buoy 45142. (c) As in Fig. 3a but for buoy 45005

(b)

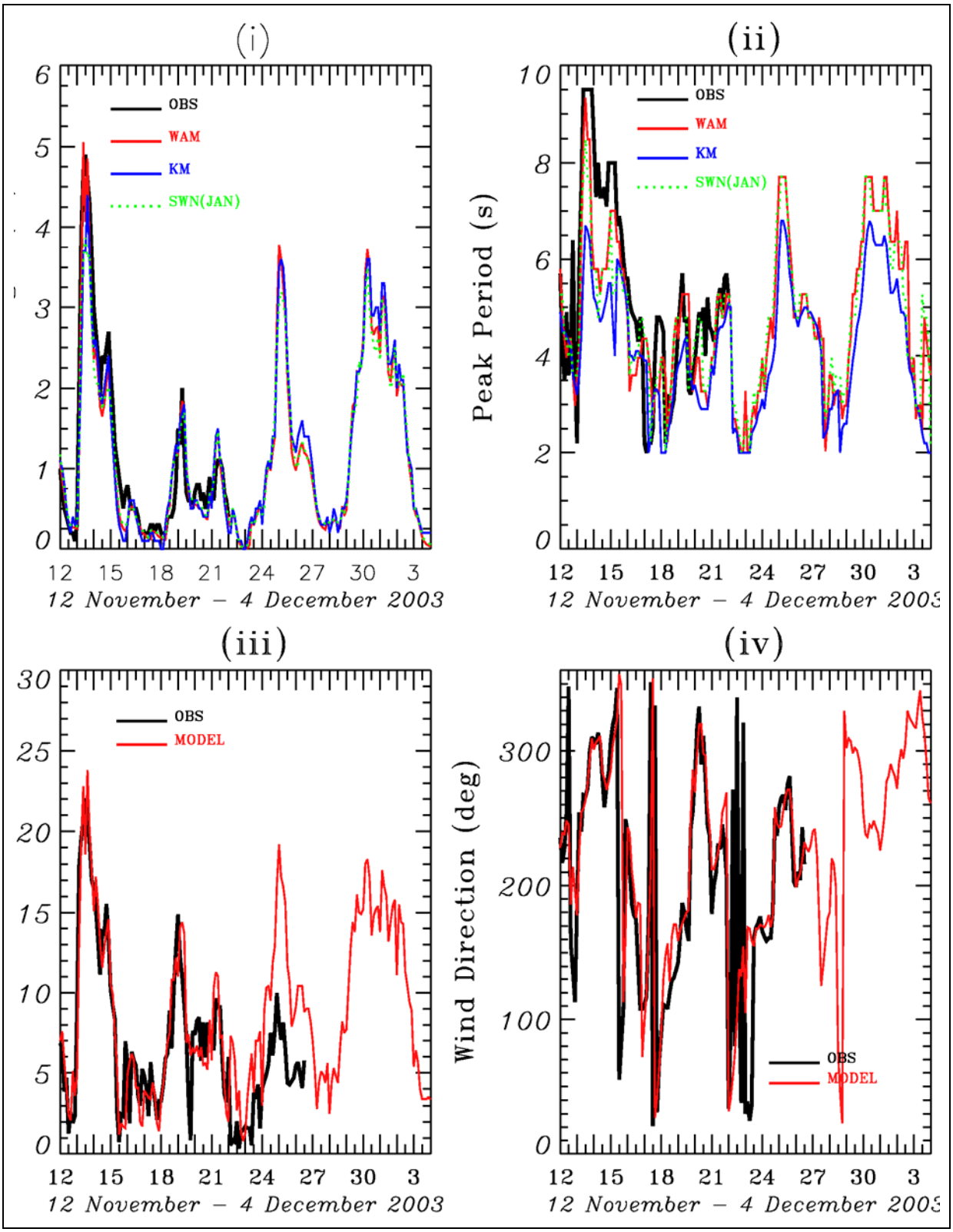

Fig. 3 Continued.

(c)

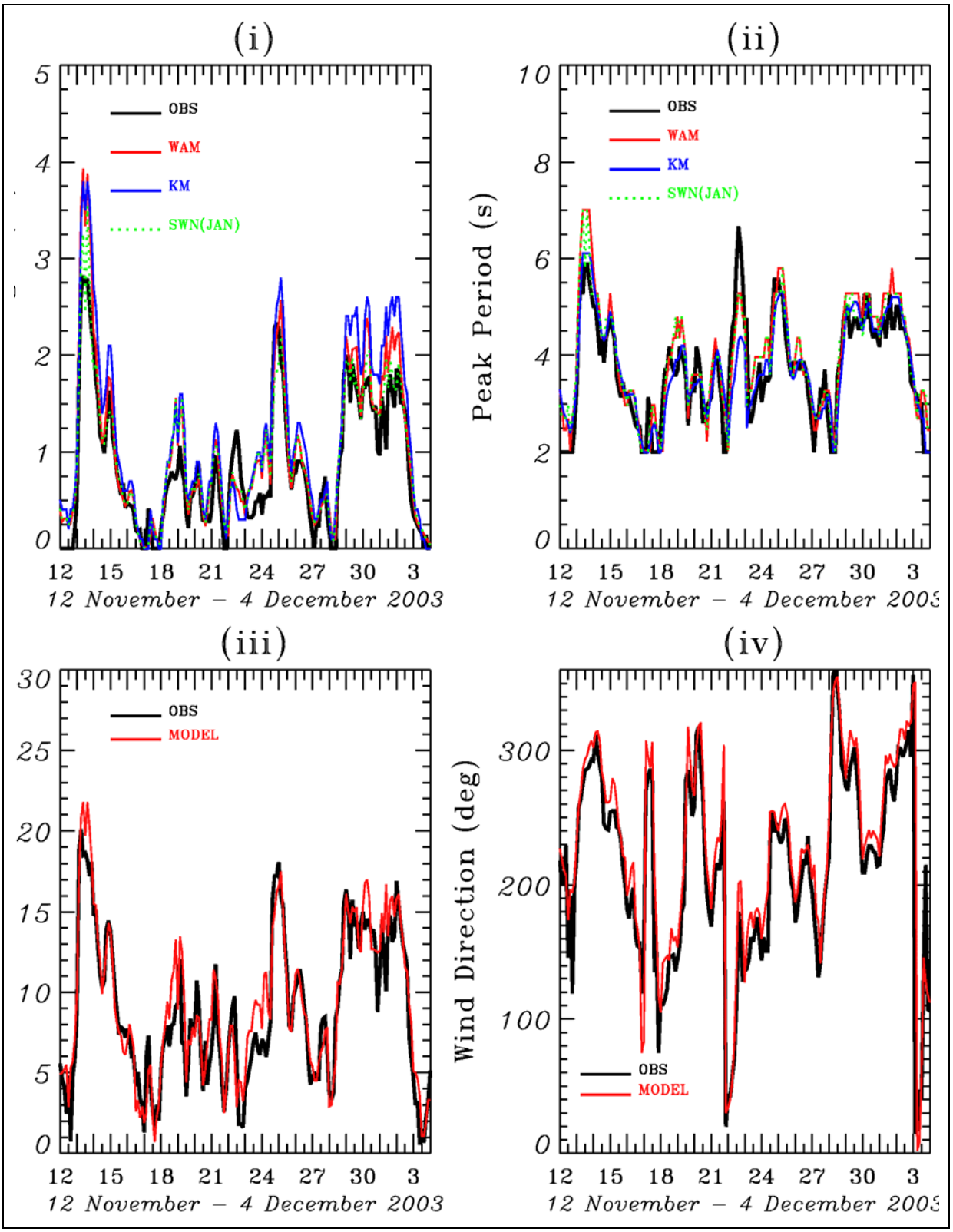

Fig. 3 Continued.

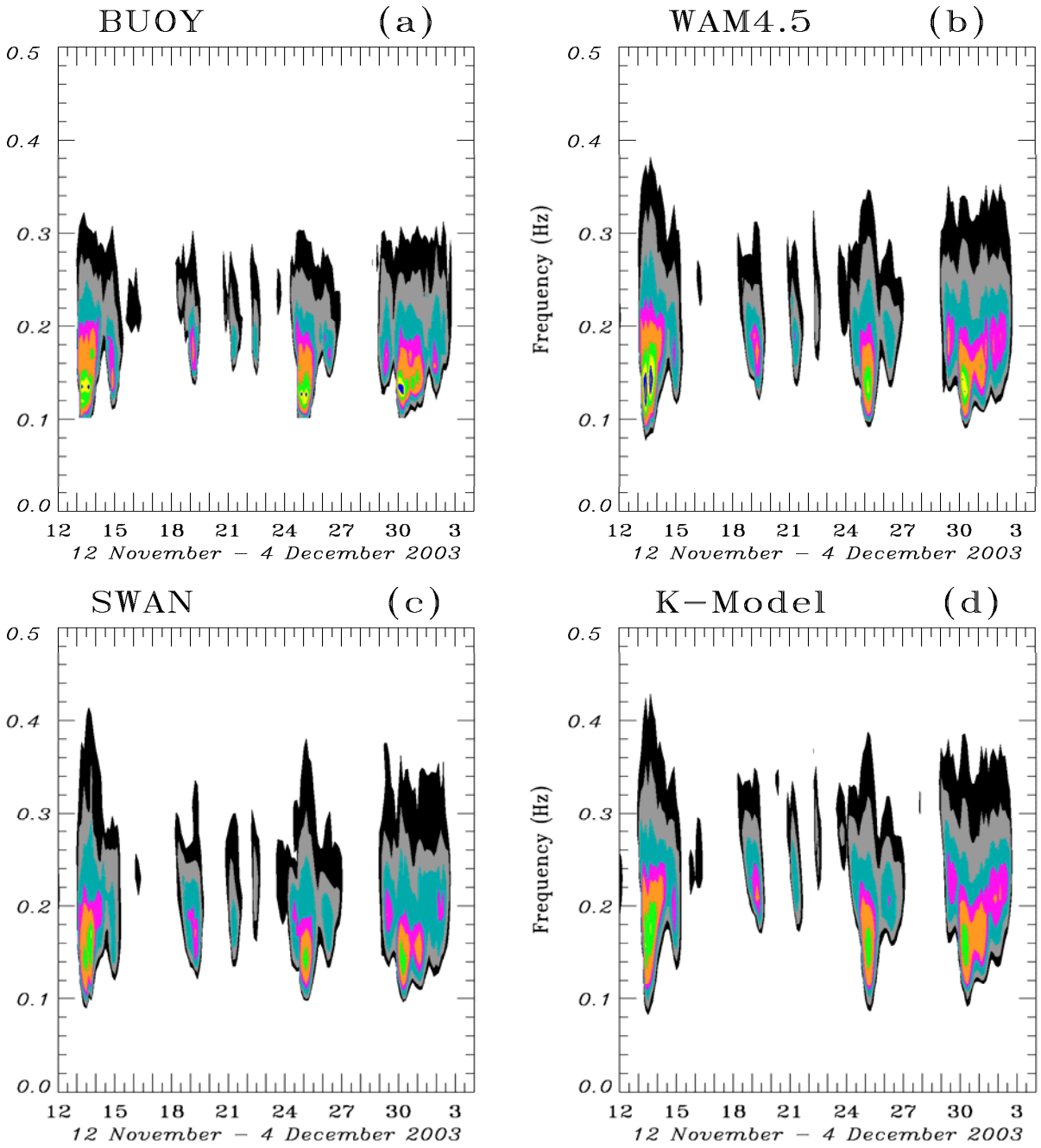

Fig. 4 Time series plots of the buoy and modelled one-dimensional spectra at 3-hour intervals at the location of buoy 45132 for the period 12 November - 4 December 2003. The spectra shown are (a) buoy, (b) the WAM4.5 run, (c) the SWAN run and (d) the K-model run. The coloured areas are energy density levels in m^2 Hz^{-1}, namely, black (0.25 – 0.5), grey (0.5 - 1.0), turquoise (1.0 - 2.0), pink (2.0 - 3.0), orange (3.0 – 6.0), green (6.0 – 9.0), yellow (9.0 – 12.0), blue (12.0 – 15.0), kaki (15.0 – 18.0) and red (18.0 – 21).

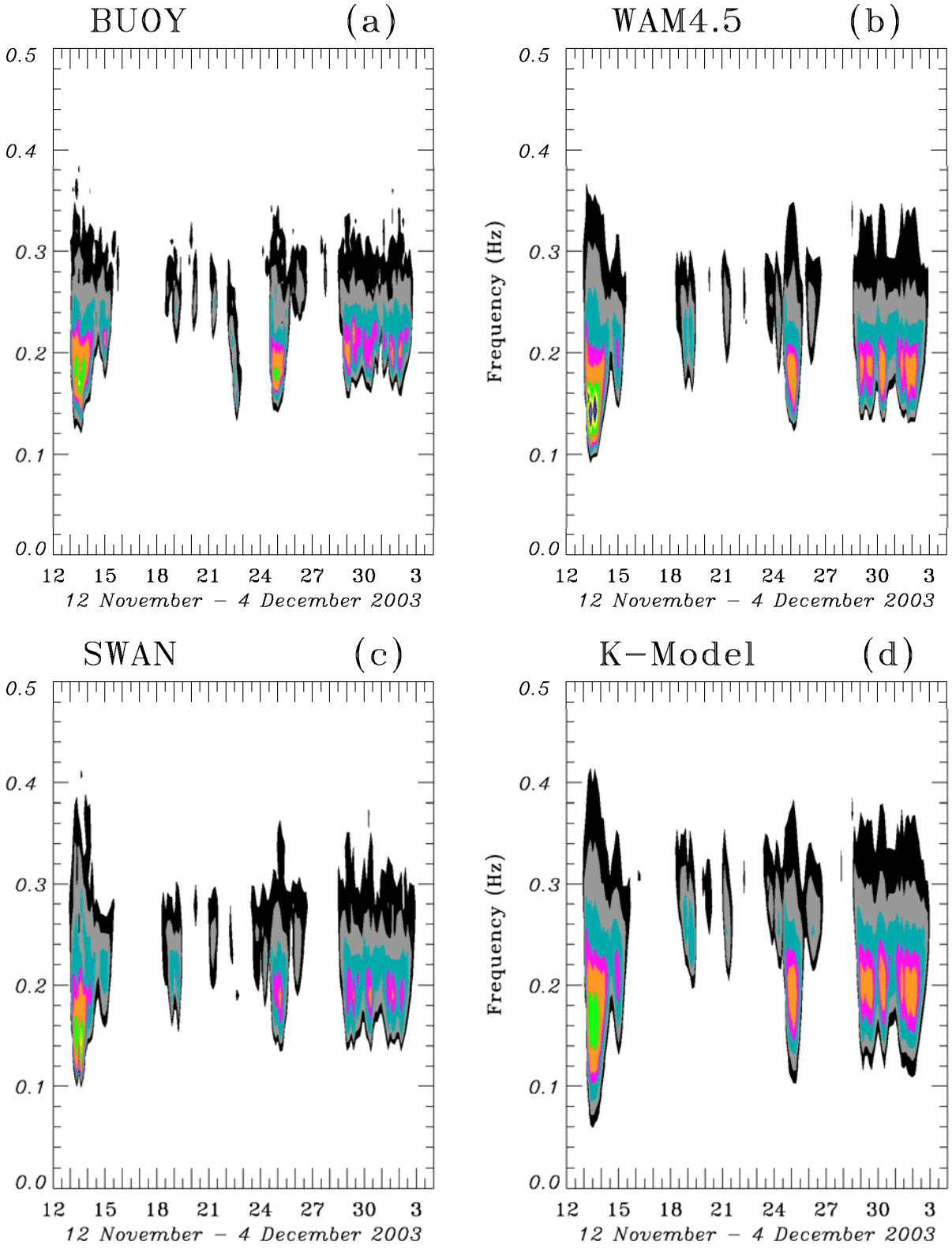

Fig. 5 As in Fig. 4 but for buoy 45005

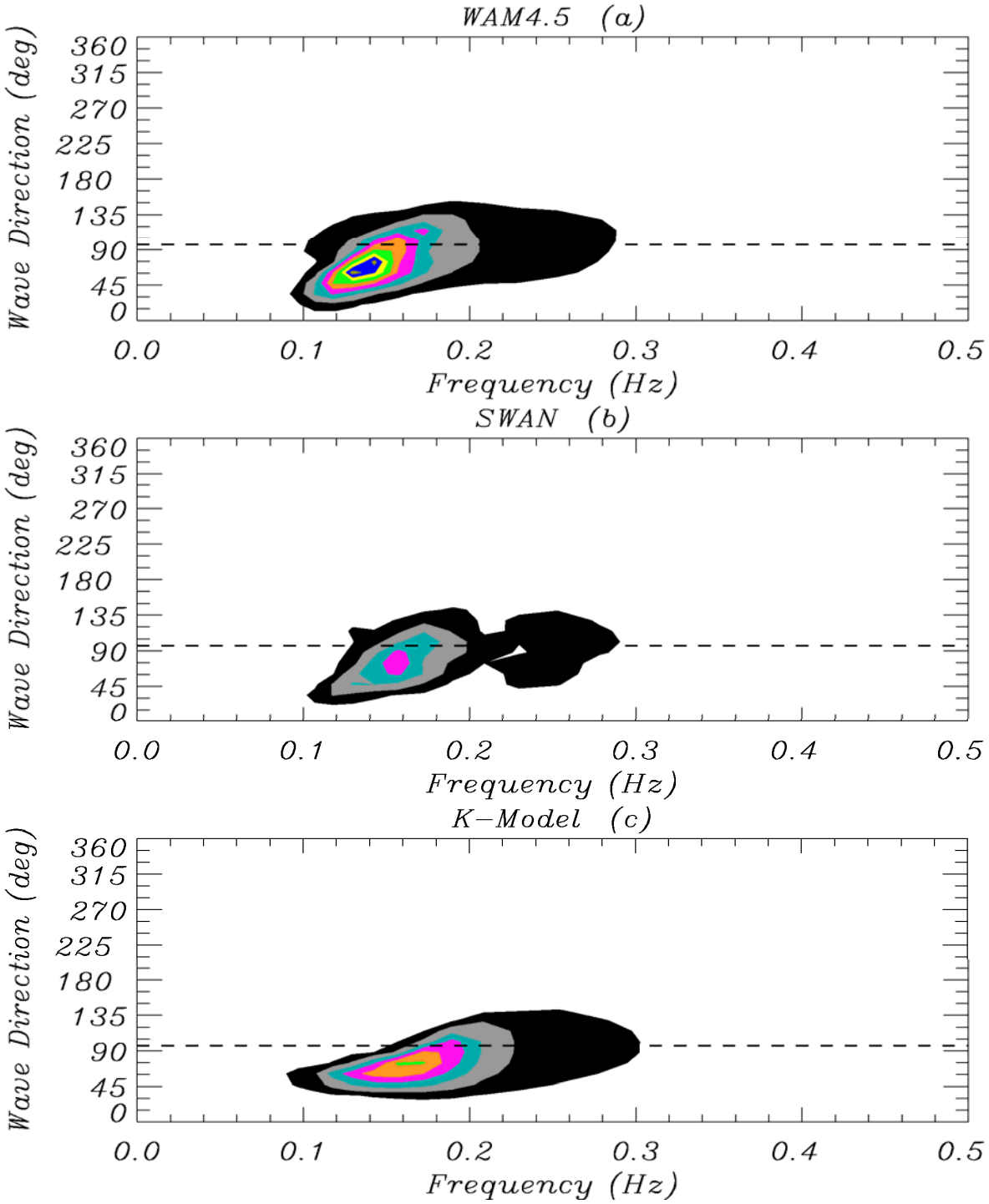

Fig. 6 Modelled two-dimensional wave spectra valid at 1500 UTC 13 November 2003 at buoy location 45132. The dashed line is the direction to which the wind is blowing at that time. The coloured areas are spectral energy density levels in m^2 Hz^{-1} rad^{-1}, namely, black (0.5 – 2.0), grey (2.0 - 4.0), turquoise (4.0 - 6.0), pink (6.0 - 8.0), orange (8.0 – 10.0), green (10.0 – 12.0), yellow (12.0 – 14.0), blue (14.0 – 16.0), kaki (16.0 – 18.0) and red (18.0 – 20).

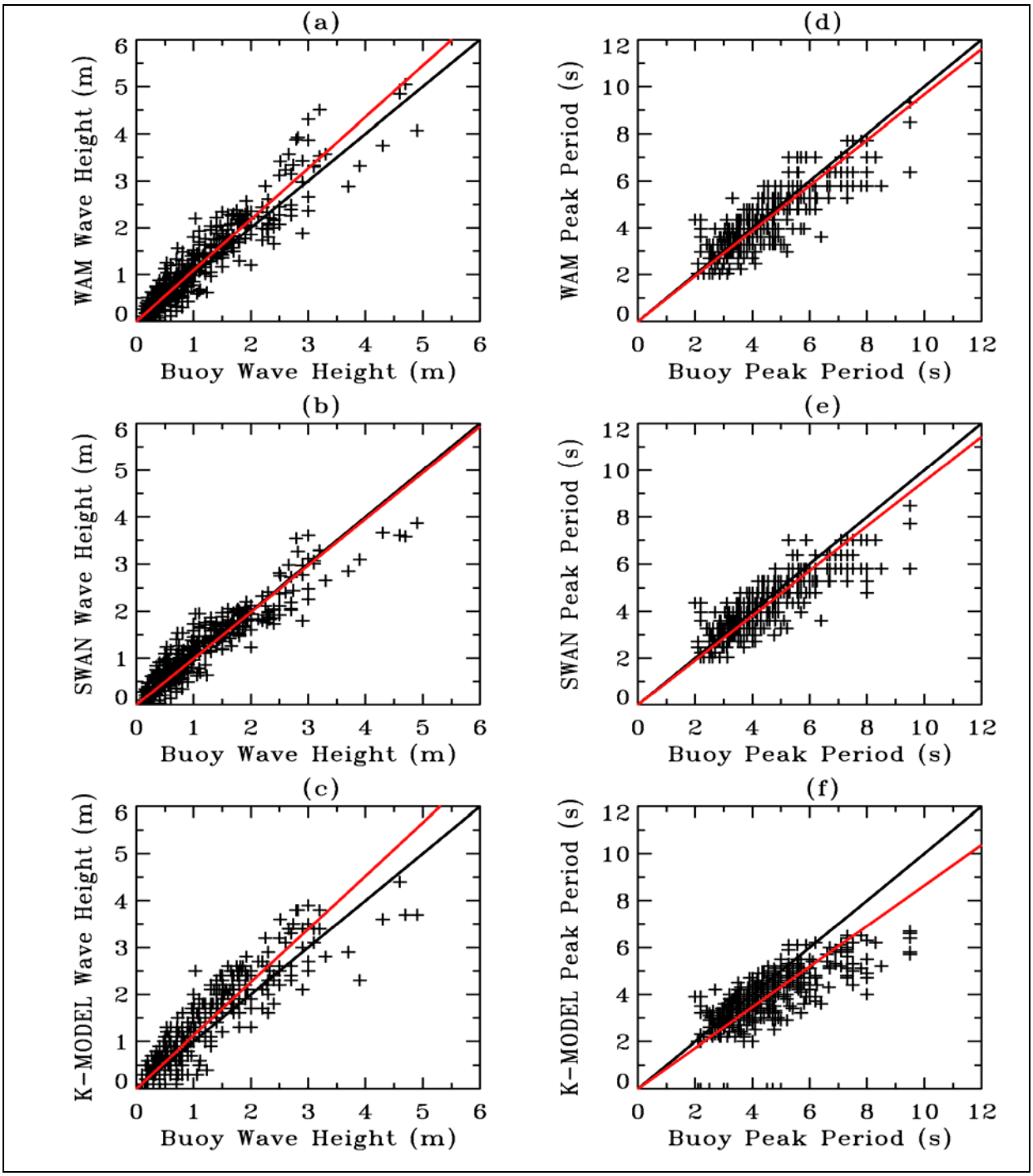

Fig. 7 Scatter plots of modelled versus observed wave heights and peak periods at buoys based on observations at buoys 45005, 45132 and 45142 for the time period 12 November – 4 December 2003. The black lines denote the perfect fit to model and observed values and the red lines the symmetric slope s, as defined in the appendix. Model values are overpredicted for $s > 1.0$ and underpredicted for $s < 1.0$.

Table 1: Source term, growth limiter and depth refraction options included in each of the three wave models used in this study.

Options	Reference	Wave Models		
		WAM4.5	SWAN	K-Model
S_{phil}	Cavaleri and Malanotte-Rizzoli (1981)	x	x	x Modified See eq. 16
S_{in}	Komen et al. (1984); WAMDI Group (1988) Janssen (1989, 1991)	x	x Modified See text	x Modified See eqs. (17)–(19)
S_{nl4}	Hasselmann et al. (1985)	x	x	Neglected
S_{nl3}	Eldeberky (1996)		Not activated	
S_{ds}	Janssen (1989, 1991) Schneggenburger (2000); Schneggenburger et al (1998)	x	x	x (See eqs. (20)–(21)
S_{bf} Dissipation const. (m^2s^{-3})	Hasselmann et al. (1973)	x 0.038	x 0.038	x 0.038
S_{br}	Battjes and Janssen (1978)	Not activated	Not activated	Implicit inclusion in S_{ds}
Growth limiter	Hersbach and Janssen (1999)	x	x	x
Depth refraction		x	x	x

Table 2: The CPU time and propagation and integration time steps used by each of the three models. The three models use the same computer system which is a LINUX machine with one CPU.

	WAM4.5	**SWAN**	**K-MODEL**
CPU time (s)	**5450**	**11400**	**12900**
Propagation time step (s)	**120**	**1200**	**180**
Integration time step (s)	**720**	**1200**	**720**

Table 3: Validation statistics for significant wave heights >= 0.1 m for the time period 12 November – 4 December 2003 for the different wave model runs (SI: Scatter index, r: linear correlation coefficient, ac: anomaly correlation, rv: reduction of variance, s: symmetric slope and N: number of observations). The mathematical definitions of the statistical parameters are given in the Appendix

H_s (m)	WAM4.5	SWAN	K-Model
buoy mean	**1.043**	**1.043**	**1.043**
model mean	**1.136**	**1.076**	**1.204**
bias	**0.093**	**0.033**	**0.161**
stddev	**0.319**	**0.291**	**0.376**
SI	**0.305**	**0.279**	**0.361**
r	**0.938**	**0.938**	**0.912**
ac	**0.927**	**0.934**	**0.890**
rv	**0.844**	**0.879**	**0.764**
s	**1.089**	**0.989**	**1.131**
N	**412**	**412**	**412**

Table 4: Same as Table 3 but for peak periods >= 2.0 seconds.

T_p (seconds)	WAM4.5	SWAN	K-Model
buoy mean	**4.591**	**4.591**	**4.591**
model mean	**4.479**	**4.441**	**4.008**
bias	**-0.112**	**-0.150**	**-0.583**
stddev	**0.778**	**0.773**	**0.973**
SI	**0.169**	**0.168**	**0.212**
r	**0.846**	**0.850**	**0.745**
ac	**0.834**	**0.839**	**0.704**
rv	**0.717**	**0.716**	**0.409**
s	**0.967**	**0.952**	**0.864**
N	**411**	**411**	**411**

Table 5: Validation statistics for buoy wind speeds at 10 m level (U_{10}) >= 2.0 ms^{-1} for the time period 12 November – 4 December 2003. The wind field input is the same for each model. (SI: Scatter index, r: linear correlation coefficient, ac: anomaly correlation, rv: reduction of variance, s: symmetric slope and N: number of observations). The mathematical definitions of the statistical parameters are given in the Appendix

U_{10} (ms^{-1})	**MODEL**
buoy mean	8.920
model mean	9.369
bias	0.449
stddev	2.232
SI	0.250
r	0.889
ac	0.873
rv	0.750
s	1.055
N	443